# A chemical proteomic strategy reveals inhibitors of lipoate salvage in bacteria and parasites

Dienemann, J.N.; Chen, S.Y.; Hitzenberger, M.; Sievert, M.L.; Hacker, S.M.; Prigge, S.T.; ... ; Sieber, S.A.

How to cite: *Angew. Chem. Int. Ed.* **2023**, *62*, e202304533
doi.org/10.1002/anie.202304533

**Proteomics** **Hot Paper**

# A Chemical Proteomic Strategy Reveals Inhibitors of Lipoate Salvage in Bacteria and Parasites

*Jan-Niklas Dienemann, Shu-Yu Chen, Manuel Hitzenberger, Montana L. Sievert, Stephan M. Hacker, Sean T. Prigge, Martin Zacharias, Michael Groll, and Stephan A. Sieber**

**Abstract:** The development of novel anti-infectives requires unprecedented strategies targeting pathways which are solely present in pathogens but absent in humans. Following this principle, we developed inhibitors of lipoic acid (**LA**) salvage, a crucial pathway for the survival of **LA** auxotrophic bacteria and parasites but non-essential in human cells. An **LA**-based probe was selectively transferred onto substrate proteins via lipoate protein ligase (LPL) in intact cells, and their binding sites were determined by mass spectrometry. Probe labeling served as a proxy of LPL activity, enabling in situ screenings for cell-permeable LPL inhibitors. Profiling a focused compound library revealed two substrate analogs (**LAMe** and **C3**) as inhibitors, which were further validated by binding studies and co-crystallography. Importantly, **LAMe** exhibited low toxicity in human cells and achieved killing of *Plasmodium falciparum* in erythrocytes with an $EC_{50}$ value of 15 μM, making it the most effective LPL inhibitor reported to date.

## Introduction

Cofactors enhance the scope of chemical transformations in enzymes beyond the limited diversity provided by the 20 canonical amino acids.[1] They play crucial roles in many cellular processes and are thus attractive drug targets.[2] Recently, several chemical proteomic strategies utilized small molecule cofactor mimics, e.g. pyridoxal phosphate[3] and heme,[4] to infiltrate the cellular metabolic machinery and facilitate their incorporation in cofactor-dependent enzymes. A small bioorthogonal handle (alkyne or azide) is clicked to an affinity tag (e.g., biotin) for enrichment on avidin beads and subsequent identification by mass spectrometry (MS).[5] In addition to the discovery of previously unknown cofactor-dependent enzymes, the methodology identified inhibitors against selected targets via competitive profiling.[6]

Lipoic acid (**LA**) is a promising candidate for this strategy as it contributes to central metabolism in various organisms.[7] **LA** is covalently bound to particular lysine residues where it catalyzes reactions such as acyl-CoA formation in dehydrogenase complexes, e.g., pyruvate dehydrogenase (oxidative decarboxylation).[8] Bacteria and parasites exhibit a highly diverse machinery to synthesize or acquire the cofactor compared to humans. In *Escherichia coli*, the biosynthesis pathway consists of the enzymes LipB (octanoyl transferase) and LipA (lipoyl synthase). These enzymes assemble the **LA** cofactor directly ('on-site') on specific lysine residues of conserved domains of **LA**-dependent proteins via octanoylation (LipB) and subsequent introduction of the redox-active dithiolane moiety (LipA, Figure 1A).[7a,b,d] In addition, salvage of **LA** is an alternate strategy by which organisms lipoylate proteins with the scavenged cofactor from the exterior environment (Figure 1A). This process is catalyzed by ATP-dependent lipoate protein ligases (LPL).[7a,b,d,9] By contrast, no homologous **LA** salvage pathway is known in mammalian cells, which instead rely on **LA** biosynthesis in the mitochondrion.[7a,d,10] Some bacteria and parasites, such as *Listeria monocytogenes*[11] and *Plasmodium* spp.,[12] respectively, are **LA** auxotroph organisms, i.e., they rely on the uptake and salvage of **LA** for survival (in case of *P. falciparum* and *P. berghei* into the mitochondrion). Thus, these organisms represent a unique opportunity for the development of selective LPL inhibitors in order to block **LA**-dependent central metabolism pathways and, thereby, growth.[13] Despite this intriguing opportunity and the urgent need for novel anti-infectives, the development of such inhibitors has not been significantly

[*] J.-N. Dienemann, S.-Y. Chen, M. Hitzenberger, M. Zacharias, M. Groll, S. A. Sieber
Technical University of Munich, TUM School of Natural Sciences, Department of Bioscience, Center for Functional Protein Assemblies (CPA)
Ernst-Otto-Fischer Strasse 8, 85748 Garching bei München (Germany)
E-mail: stephan.sieber@tum.de

M. L. Sievert, S. T. Prigge
Department of Molecular Microbiology and Immunology, Johns Hopkins Bloomberg School of Public Health
615N. Wolfe Street, E5132, MD 21205 Baltimore, (USA)

S. M. Hacker
Leiden Institute of Chemistry, Leiden University
Einsteinweg 55, 2333CC Leiden (The Netherlands)

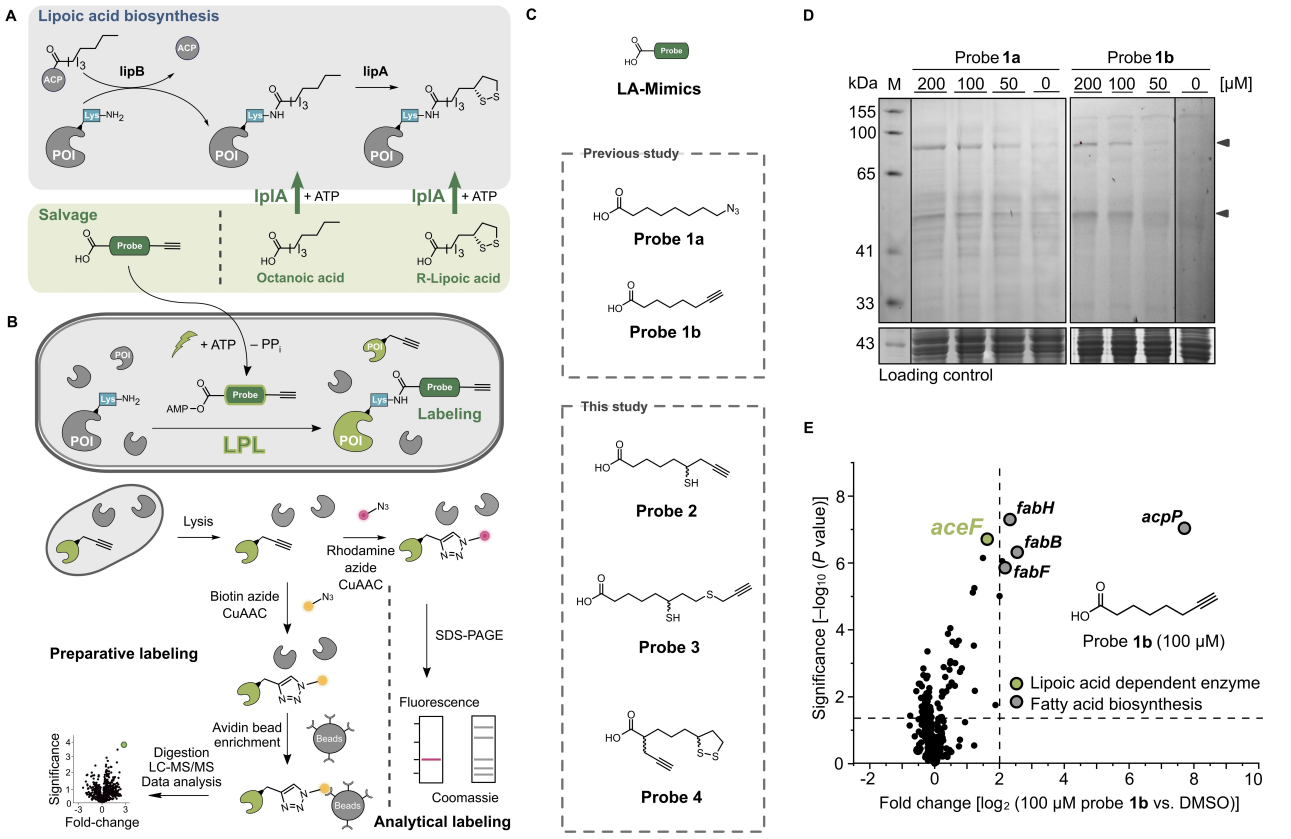


***Figure 1.*** In situ chemical proteomic strategy to investigate lipoylation via LPL-mediated activation and transfer. A) The biosynthesis (grey box) and salvage of **LA** (green box) via the LPL enzyme lplA in *E. coli*. ACP—acyl carrier protein, POI—protein of interest. B) Intracellular probe-based infiltration strategy via ATP-dependent LPL as **LA** salvage enzyme with subsequent downstream analysis of labeled proteins by click-chemistry (CuAAC—copper-catalyzed azide-alkyne cycloaddition) using either gel-based rhodamine fluorescence readout by SDS-PAGE (magenta, analytical labeling) or mass spectrometry-based detection after biotin conjugation and enrichment on avidin beads (yellow, preparative labeling). C) Probe structures as **LA** salvage mimics used in this study. D) Analytical labeling of intact *E. coli* Δ*lipB* cells with probes **1a** and **1b** (2 h) in stationary phase revealed a similar pattern of concentration-dependently labeled fluorescent bands (grey arrows). The procedure with the azide-bearing C8-fatty acid probe **1a** showed higher background labeling than the alkyne-based derivative **1b**.[20] "M" represents a marker as a protein size reference. Coomassie staining served as loading control. E) The volcano plot shows enrichment of mainly fatty acid biosynthesis proteins (grey) on a $\log_2$ scale after treatment of intact *E. coli* Δ*lipB* cells in stationary phase with the alkyne-bearing probe **1b** (100 μM, 2 h). Of note, the **LA**-dependent protein product of the gene *aceF* (green) could be 3-fold enriched. The threshold lines indicate 4-fold enrichment compared to DMSO and a $-\log_{10}$ *P* value of 1.3 (two-sided two-sample *t*-test, $n = 4$ independent experiments per group). Gene names of proteins are shown in italic.

exploited. One example is the redox-inactive small molecule mimic of **LA**, 8-bromo octanoic acid (**BrO**), which is transferred via LPL to substrate proteins, but cannot further support enzymatic catalysis.[14] **BrO** was shown to reduce growth of *P. falciparum* in erythrocytes,[12a] *P. berghei* in HepG2 cells[12b] and mice,[15] and *Toxoplasma gondii* in fibroblasts,[16] but high concentrations up to the millimolar range were needed for parasite killing.[12,15] Thus, novel chemical tools are required to decipher more potent LPL inhibitors. Recently, two methods have been introduced to chemically modify endogenous lipoylated proteins exclusively in lysates via iodoacetamide-assisted lipoate-cyclooctyne ligation (iLCL)[17] or reduction of the dithiolane ring followed by thioacetalization with an alkynylated aldehyde.[18] These methods enriched lipoylated proteins in lysates and determined their lipoylation sites on lysines. However, because they do not involve the transfer of **LA** via LPL catalysis in intact cells, they are unsuitable for direct inhibitor discovery via competitive profiling.

Here, we introduce novel **LA** probes, which infiltrate the cellular salvage pathway in intact cells and get incorporated in cognate lipoate-dependent proteins (Figure 1B).

Chemical proteomics of intact *E. coli* and *L. monocytogenes* cells show selective enrichment of **LA**-dependent proteins and resolution of their modified lysine sites. Computational design, in situ profiling, and co-crystallization revealed two effective LPL inhibitors (**C3** and **LAMe**). These compounds killed *P. falciparum* in erythrocytes with $EC_{50}$ values of 27 μM and 15 μM, respectively, highlighting the value of this approach in uncovering novel anti-infectives.

## Results and Discussion

### Design and Synthesis of Probes to Monitor Protein Lipoylation

As benchmarks, we started our studies with the C8-fatty acid probes **1a** (8-azido octanoic acid) and **1b** (7-octynoic acid) as previously confirmed LPL substrates (Figure 1C).[19] First, we determined their toxicity in *E. coli* and identified up to 50 % growth reduction with probe **1a**, while probe **1b** showed no effect (Figure S1A). Next, wild-type *E. coli* and Δ*lipB* cells, bearing a mutation in the de novo biosynthesis pathway to maximize probe uptake, were treated with various concentrations of the non-toxic probe **1b** for 2 h in the stationary and exponential phase. Cells were lysed and click-chemistry was used to link any proteins modified by probe **1b** to rhodamine azide for fluorescent SDS-PAGE analysis (Figure 1B). Interestingly, a distinct labeling pattern was only observed in the stationary phase of Δ*lipB* cells at a probe concentration of 50 μM or higher (Figure 1D, S1B). A similar fluorescence pattern with higher background labeling was observed for the azide-bearing probe **1a** after linking modified proteins to rhodamine alkyne by click-chemistry.[20] From these results, we selected optimal conditions to perform quantitative MS analysis of covalently-labeled proteins. Therefore, we treated stationary cells for 2 h with 100 μM of the non-toxic probe **1b**, followed by lysis, click to biotin azide, enrichment, digestion, and analysis via LC–MS/MS (Figure 1B). Notably, one of the three **LA**-dependent proteins known in *E. coli*, ODP2 (*aceF*), was 3-fold enriched (Figure 1E).[17,18] Moreover, numerous proteins belonging to fatty acid biosynthesis were among the top hits [$-\log_{10}$ (*P* value) 6–8, $\log_2$ (fold-change) 2–8]. These initial results demonstrated the infiltration of bacterial **LA** metabolism. However, the relatively simple probe design prevented the desired specificity for **LA**-dependent proteins with fatty acid biosynthesis enzymes as predominant off-targets.

In order to enhance the fidelity in detection of enzyme lipoylation, we designed a suite of **LA** mimics as probes that are attainable by chemical synthesis (Figure 1C). Starting from probe **1b**, we incrementally increased the structural complexity to more closely mimic **LA**. In a first step, we placed a free thiol at position 6 of 8-nonynoic acid to obtain probe **2**. The synthesis started with propargylating cyclohexanone (**5**), followed by a Baeyer–Villiger oxidation as a key step to introduce the lactone moiety (Scheme 1).[21] After ring opening by transesterification, the hydroxyl group at position 6 could be transformed into thioester **10** by tosylation and substitution with thioacetate. Saponification as final step generated probe **2** as a racemic mixture in six steps (5 % overall yield).

Next, the propargyl tag was linked to the thiol at position 8 of the reduced **LA** moiety as a thioether (probe **3**). Probe **4** presents the most similar mimic to **LA** after functionalization at position 2 with a propargyl handle. For probes **3** and **4**, **LA** was protected by esterification, followed by reduction to open the dithiolane ring. To obtain probe **3**, the thiol group at position 8 was selectively propargylated, followed by saponification to liberate the carboxylic acid as racemate. By contrast, for probe **4**, both thiols were protected by tritylation to install a propargyl tag at position 2, followed by global deprotection and oxidation to yield the desired probe as a mixture of all diastereoisomers (Scheme S1).

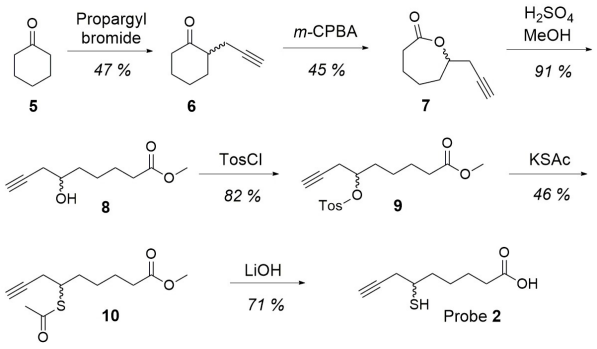


***Scheme 1.*** Synthesis of probe **2**. The propargylated lactone **7** was synthesized as previously reported[21] prior to transesterification (**8**), tosylation (**9**), and nucleophilic substitution by thioacetate. Global saponification of **10** yielded probe **2** as racemate.

### Probe 2 Labels LA-dependent Proteins in *E. coli* and *L. monocytogenes*

With a panel of probes (**2**–**4**) in hand, we first tested their impact on bacterial growth under labeling conditions (Figure S2A). At high concentrations of 500 μM, only probe **2** slightly reduced the growth of *E. coli* Δ*lipB* by 20 %. Secondly, we examined their labeling performance in intact *E. coli* Δ*lipB* cells in both fluorescent gel-based and LC–MS/MS experiments. Labeling with probes **4** and **3** revealed high background without competition upon **LA** treatment (Figure S2B, C). However, probe **2** showed distinct bands on the fluorescent gel that could be competed with **LA** and **BrO** pre-treatment, indicating that **LA**-dependent proteins were labeled via LPL (Figure 2A). Additionally, application of probe **2** in wild-type *E. coli* cells showed no labeling indicating that it cannot compete with the de novo biosynthesis (Figure S2D). Subsequent quantitative LC–MS/MS profiling exclusively revealed all three known **LA**-dependent enzymes in the *E. coli* Δ*lipB* cells (ODP2—*aceF*, 66 kDa; ODO2—*sucB*, 44 kDa; GCSH—*gcvH*, 14 kDa) without any background (Figure S3A).[17,18] Moreover, labeling was competed by addition of **LA** or **BrO** in 10-fold excess, demonstrating improved specificity of probe **2** (Figure 2B, S3B).

To rationalize the diverging labeling properties, we applied computational methods to predict how **LA** and the probe stereoisomers bind into the crystal structure of *E. coli* LPL (lplA—*lplA*, PDBID 1x2h).[22] The structures were docked into the active site (Figure S4A) and subjected to molecular dynamics (MD) simulations to investigate their binding behavior, including binding free energies ($\Delta\Delta G_{Bind}$), root-mean-square deviation ($RMSD_{Lig}$), and root-mean-square fluctuation ($RMSF_{Lig}$). Different binding modes were observed across these compounds. The *S*-enantiomer of

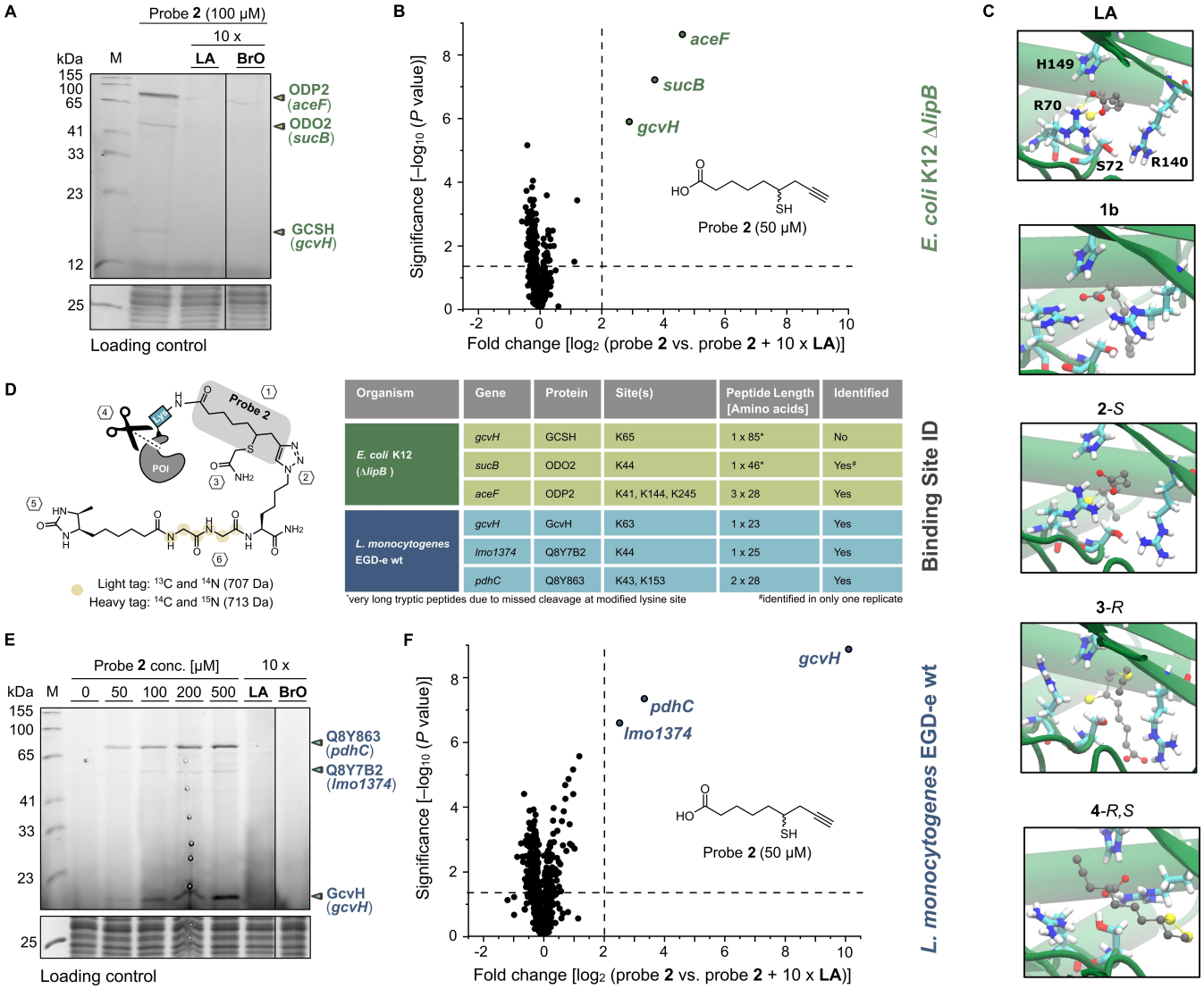


***Figure 2.*** In situ profiling of lipoylation in *E. coli* Δ*lipB* (Gram-negative) and *L. monocytogenes* wild type (Gram-positive) with binding site identification. Gene names of corresponding protein products are presented in italic. "M" represents a marker as a protein size reference, and Coomassie staining served as loading control during analytical labeling. Of note, the protein products might show reduced migration on SDS-PAGE after rhodamine modification. The threshold lines in volcano plots indicate a $-\log_{10} P$ value of 1.3 (two-sided two-sample *t*-test, $n=4$ independent experiments per group) and 4-fold enrichment. A) Analytical labeling of intact *E. coli* Δ*lipB* cells with probe **2** (100 µM, 2 h) and in competition with 10-fold excess (1 mM) of **LA** or **BrO** indicated infiltration of **LA** salvage via LPL. The green arrows mark the expected size of ODP2 (*aceF*, 66 kDa), ODO2 (*sucB*, 44 kDa), and GCSH (*gcvH*, 14 kDa) as known lipoylated proteins.[17,18] B) The volcano plot presents preparative labeling results of intact *E. coli* Δ*lipB* cells with probe **2** (50 µM, 2 h) in comparison to probe **2** (50 µM) in competition with 10-fold excess **LA** (500 µM), indicating selective enrichment of **LA**-dependent enzymes.[17,18] C) Representative snapshots of the native *R*-enantiomer of **LA** and computationally predicted best-performing probe candidates **1b**, **2**-*S*, **3**-*R* and **4**-*R*,*S* in *E. coli* lplA (PDBID 1x2h) are depicted at the end of molecular dynamics simulations (400 ns), highlighting comparable binding orientations of **LA** and **2**-*S* in contrast to **1b**, **3** and **4** (Figure S4B–D). D) The methodology of isoDTB tags[23] was applied to identify the binding sites of probe **2** on lysine residues in *E. coli* Δ*lipB* and *L. monocytogenes* that corresponded to protein lipoylation sites. After labeling respective lysines in intact bacterial cells with probe **2** (1), the labeled proteome was clicked to a heavy and a light isoDTB tag as a technical replicate (2), followed by capping of free thiols with iodoacetamide (3). Proteins were digested by trypsin (4) to release the modified desthiobiotinylated peptides with one missed cleavage at the modified lysine. Tryptic peptides were enriched on avidin beads (5) and eluted to be identified by mass spectrometry. Mass shifts of 707 Da and 713 Da revealed isoDTB-tagged peptides (6). Peptides up to 28 amino acids were detected without problems in contrast to longer tryptic peptides with missed cleavage at the modified lysine, as indicated by asterisks.[18] Peptides that were only identified in one replicate were marked with #. E) Concentration-dependent analytical labeling of intact *L. monocytogenes* wild type cells with probe **2** (0 µM–500 µM, 2 h) and competition with 10-fold excess (2 mM) of **LA** or **BrO** compared to probe **2** (200 µM) revealed infiltration of **LA** salvage via LPL and lipoyl transferase LipL. The blue arrows mark the expected size of Q8Y863 (*pdhC*, 58 kDa), Q8Y7B2 (*lmo1374*, 45 kDa), and GcvH (*gcvH*, 14 kDa) as known **LA**-dependent proteins.[24] (F) The volcano plot presents preparative labeling results of intact *L. monocytogenes* wild type cells with probe **2** (50 µM, 2 h) in comparison to probe **2** (50 µM) in competition with 10-fold excess **LA** (500 µM), indicating selective enrichment of **LA**-dependent enzymes.[24]

probe **2** exhibited similar binding stability as **LA**, shown by $RMSD_{Lig}$ and $RMSF_{Lig}$ (Figure S4B), and both compounds remain in a binding pose forming hydrogen bonds with R70, H149, and S72 (Figure 2C, S4C). By contrast, probe **1b** and enantiomers and diastereomers of probes **3** and **4**, respectively, were occasionally attracted by neighboring R140 and deviated from their initial binding locations (Figure 2C, S4B–D), which may prevent their activation by ATP for subsequent transfer to **LA**-dependent proteins (Figure 1B).

With probe **2** as ideal lipoylation tool in hand, we deciphered the modified lysines in whole *E. coli* proteomes. Enrichment of the labeled peptides via tailored desthiobiotin (isoDTB) linkers[23] and subsequent MS analysis revealed K44 of ODO2 (*sucB*) and K41/K144/K245 of ODP2 (*aceF*) as modified lipoylation sites, which is in line with literature data (Figure 2D).[17,18]

The high fidelity of our method was also retained when we switched from the Gram-negative *E. coli* mutant to the labeling of a wild-type Gram-positive *L. monocytogenes* bacterial strain, which relies solely on an **LA** salvage pathway consisting of two LPL orthologs (lplA1—*lmo0931*; lplA2—*lmo0764*) to lipoylate GcvH. In a next step, the lipoyl group is transferred by LipL from GcvH to other **LA**-dependent proteins.[9] Again, direct labeling of intact cells with probe **2** and competition with **LA** or **BrO** revealed three hits, comprising all known **LA**-dependent enzymes in *Listeria* (Q8Y863—*pdhC*, 58 kDa; Q8Y7B2—*lmo1374*, 45 kDa; GcvH—*gcvH*, 14 kDa; Figure 2E, F, S3C, D).[24] Additionally, the corresponding modified lysines were identified via the isoDTB technology (Figure 2D).[23] Of note, the binding sites—K63 of GcvH (*gcvH*), K44 of Q8Y7B2 (*lmo1374*) and K43/K153 of Q8Y863 (*pdhC*)—have been determined experimentally for the first time in *Listeria* and match theoretical predictions.[24]

### *Computational Design and Screen of Novel Active Site LPL Inhibitors*

The versatility of our novel labeling technology for different strains and its selectivity for the detection of lipoylated proteins represents a unique opportunity for identifying chemical compounds that lead to the manipulation of cellular lipoylation and putative therapeutic applications. Specifically, probe **2** is activated and transferred onto the cognate substrate proteins by LPL, facilitating a direct readout of its activity. The lack of an LPL-mediated salvage pathway in human cells makes this enzyme attractive for selective pathogen targeting.[9,10,12a] Since there are no active site LPL inhibitors reported, we performed computational studies to design a suite of potential candidates for subsequent validation via our competitive profiling approach using probe **2**. We initiated the inhibitor development by a structural overlay of three representative LPL enzymes, lplA from *E. coli* (Gram-negative bacterium) and LipL1 (*lipL1*) from *P. falciparum* (parasite), for which crystal structures are available,[22,25] and lplA1 from *L. monocytogenes* (Gram-positive bacterium) with a structural AlphaFold2 (AF2) prediction.[26] The overlay of all enzymes revealed a high structural similarity of the active sites as indicated by particular lysine and histidine residues (Figure S5), suggesting that inhibitors may be effective across different organisms. Three ligand binding pockets (A, B, and C, Figure S5) could be identified depending on the enzyme's catalytic state. The comparison between the **LA** bound crystal structure (*E. coli*, PDBID 1x2h, loading state)[22] and the lipoyl-AMP (**LAQ**) bound structure (*E. coli*, PDBID 3a7r, intermediate state)[25a] indicates that **LA** binds first to the initial loading pocket A (as demonstrated for the probe simulations, Figure S4) and is subsequently found in pocket B after adenylation by ATP, while the adenine motif of **LAQ** resides in pocket C. In the search for LPL active site inhibitors, we followed a two-tiered strategy by targeting pockets B and C. In the first approach, we virtually screened the ZINC database[27] by a pharmacophore-guided[28] search against the LPL active site, revealing 126 putative hits which were subsequently docked into LPL enzymes. The top 50 compounds of each ligase, selected by their docking score, were screened for overlapping compounds. The resulting 29 molecules were sorted by their averaged ranking position to identify ten commercially available compounds with the best-predicted performance (Figure S6A, B).

In a second approach, we made use of the similar catalytic activity between LPL and biotin protein ligase (BPL), for which a potent BPL inhibitor with antibacterial activity was previously reported.[29,30] This molecule, mimicking biotin-AMP as native substrate, is composed of the signature biotin moiety linked via a triazole linker to an adenine heterocycle group (Figure 3A). Both biotin and adenine bind to distinct pockets of BPL, of which the latter adenine pocket is also present in LPL (pocket C, Figure S5). We thus tailored the molecule towards LPL to mimic **LAQ** by replacing the biotin with **LA** and the triazole with a more flexible but chemically stable amide linker while preserving the same linker length (**C3**, Figure 3A). **C3** and its cropped version, lipoic acid monomethyl amide (**LAMe**, Figure 3A), were docked into the active sites of LPL from *L. monocytogenes* and *P. falciparum* in comparison to the native ligand **LA** and **BrO** (Figure 3B, S7A) to calculate and compare their binding affinities ($\Delta\Delta G_{Bind}$, Figure 3C) and stabilities ($RMSD_{Lig}$, $RMSF_{Lig}$, Figure S7B) in silico by MD simulations. Overall, the same trend of predicted binding affinities for the compounds was observed in both enzymes as follows: **C3** > **LA** ≈ **LAMe** = **BrO**. Interestingly, **LA**, **LAMe**, and **BrO** were predicted to bind stronger and more stably to pocket B of *L. monocytogenes* lplA1 (approximately $-32\ kcal\,mol^{-1}$) compared to *P. falciparum* LipL1 (roughly $-26\ kcal\,mol^{-1}$), whereas **C3** showed the strongest binding free energy with around $-38\ kcal\,mol^{-1}$ for both ligases (Figure 3C). Remarkably, the adenine motif of **C3** in pocket C of LipL1 contributed significantly to the binding free energy ($-12\ kcal\,mol^{-1}$), compared to the truncated **LAMe** solely residing in pocket B. As expected, this finding underlines a significant affinity enhancement for the introduction of the adenine-linker group in addressing both pockets. Based on these promising calculations, we synthe-

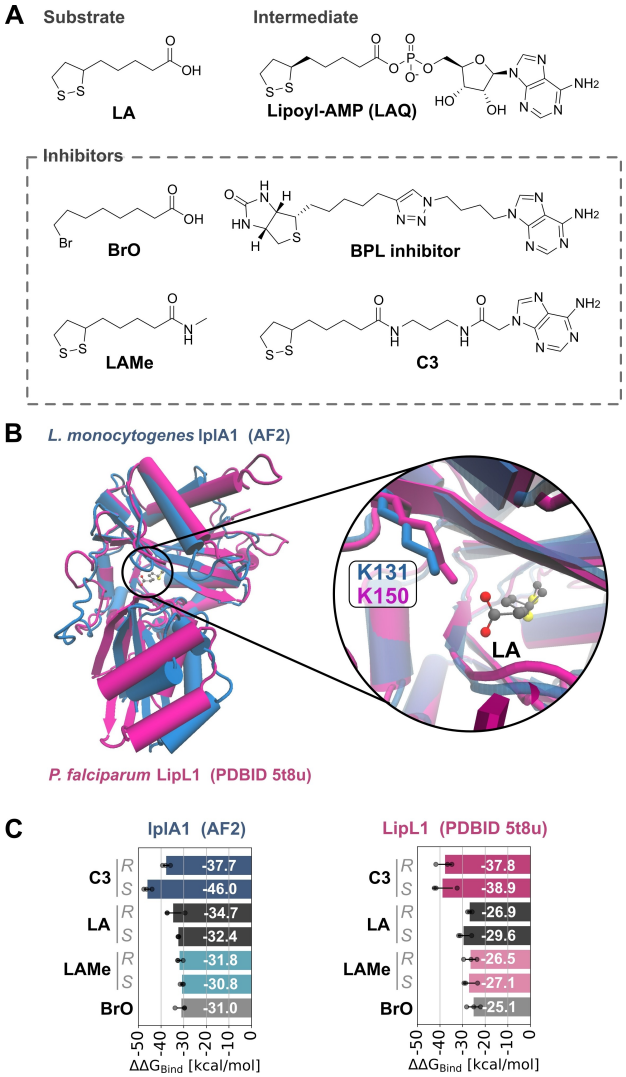


***Figure 3.*** Docking and MD simulations of rational-designed potential inhibitors of LPL in *L. monocytogenes* (blue) and *P. falciparum* (magenta) as substrate and intermediate mimics. A) The inspiration for compound design was driven by mimicking the intermediate lipoyl-AMP (**LAQ**) with chemically stable amide bonds in analogy to a previously reported inhibitor of the biotin protein ligase (BPL).[29] The simple **LAMe** molecule carries a monomethyl amide function that would not allow the **LA** moiety to be activated by ATP. **C3** presents an extended version with an additional amide linker-adenine moiety. **BrO** was described as an inhibitor of cognate lipoylation sites as it is activated and transferred by LPL.[14] **LA** as the native substrate and **BrO** as an established inhibitor serve as benchmarks. B) **LA** and all stereoisomers of potential inhibitors were docked into the active sites of *L. monocytogenes* lplA1 (AF2), and *P. falciparum* LipL1 (PDBID 5t8u), and representative binding modes of *R*-enantiomers are depicted exemplarily (Figure S7A). C) MD simulations in *L. monocytogenes* and *P. falciparum* predict all stereoisomers' LPL binding affinities ($\Delta\Delta G_{Bind}$, mean value in white). The calculations were run in $n=3$ independent attempts, and error bars represent SEM.

sized **C3** and **LAMe** by amide coupling for experimental comparison to **BrO** and **LA** (Scheme S2).

### *Biochemical and Crystallographic Studies Reveal C3 and LAMe as Active Site Inhibitors of LPL in Bacteria and Parasites*

With a suite of twelve potential LPL inhibitors at hand, we tested their performance via competitive profiling with probe **2**. For this, we focused on *L. monocytogenes* as a representative example of an **LA**-auxotrophic wild-type strain and treated cells with a 10-fold excess of competitor (1 mM) compared to the amount of probe **2** (100 μM) and analyzed the band intensity of signature protein Q8Y863 (*pdhC*, Figure 4A) via fluorescent SDS-PAGE analysis. While the ten compounds (**16**–**25**) derived from the virtual ZINC database screen largely lacked significant competition with the probe, the rationally designed **C3** and **LAMe** compounds turned out to be potent with a gel-based $EC_{50}$ value of about 210 nM and 330 nM, respectively (calculated for the residual in-gel modification of Q8Y863—*pdhC*; Figure 4B, S8A). This value is in the same range as competition with **LA** (100 nM) and 10-fold more potent than competition with the substrate analog **BrO** (2.3 μM). In addition, to verify that **C3** is an LPL inhibitor and not metabolized to release **LA** after possible enzymatic amide cleavage within the cell, we demonstrated its stability in lysate over time with an HPLC-MS-based assay (Figure S8B). In line with the lack of LPL enzymes in humans,[10a] MTT studies in HeLa cells indicate low to moderate toxicity for **LAMe** and **C3**, respectively (Figure S9A).

Accordingly, labeling with the non-toxic probe **2** (Figure S9A) in mammalian HeLa cells revealed no characteristic hits (Figure S9B). We independently confirmed a high affinity for **C3** and **LAMe** with $K_D$ values of 3.2 μM and 15 μM, respectively, which is again similar to the value of **LA** ($K_D = 1.9$ μM). By contrast, the affinity of **BrO** was very low, and hence, binding could not be quantified (Figure 4C, S10A).

Based on these results, we aimed to better rationalize the binding mode of **C3** in *L. monocytogenes* lplA1 and performed x-ray crystallography. So far, no experimental structural information of *L. monocytogenes* lplA1 is available, and we thus attempted to co-crystallize **LAQ** as the native intermediate. We noted that the C-terminus is flipped in the lplA1:**LAQ** complex (PDBID 8crj) in comparison to the predicted apo-AF2 structure (Figure S11A, B), which is in agreement with a previously co-crystallized homologous enzyme.[25a] However, the AF2 structure perfectly aligns with the co-crystals of **C3** (PDBID 8crl) and **LA** (PDBID 8cri), which confirms previous computational analysis (Figure S11B). Of note, we were able to co-crystallize **LA**, **LAQ**, and **C3** solely as *R*-enantiomers and demonstrate inhibitor binding in the active pocket as a chemically stable **LAQ** analog (Figure 4D). Interestingly, **C3** as an **LAQ** mimic could not induce the flip of the C-terminal domain (Figure S11B) as, e.g., crucial interactions with the phosphate and Lys131 are lacking, which offers a potential avenue for inhibitor refinement (Figure 4D).

Due to the structurally conserved binding pocket of *L. monocytogenes* lplA1 and *P. falciparum* LipL1 (Figure 3B, S5), we performed ITC studies with the recombinant

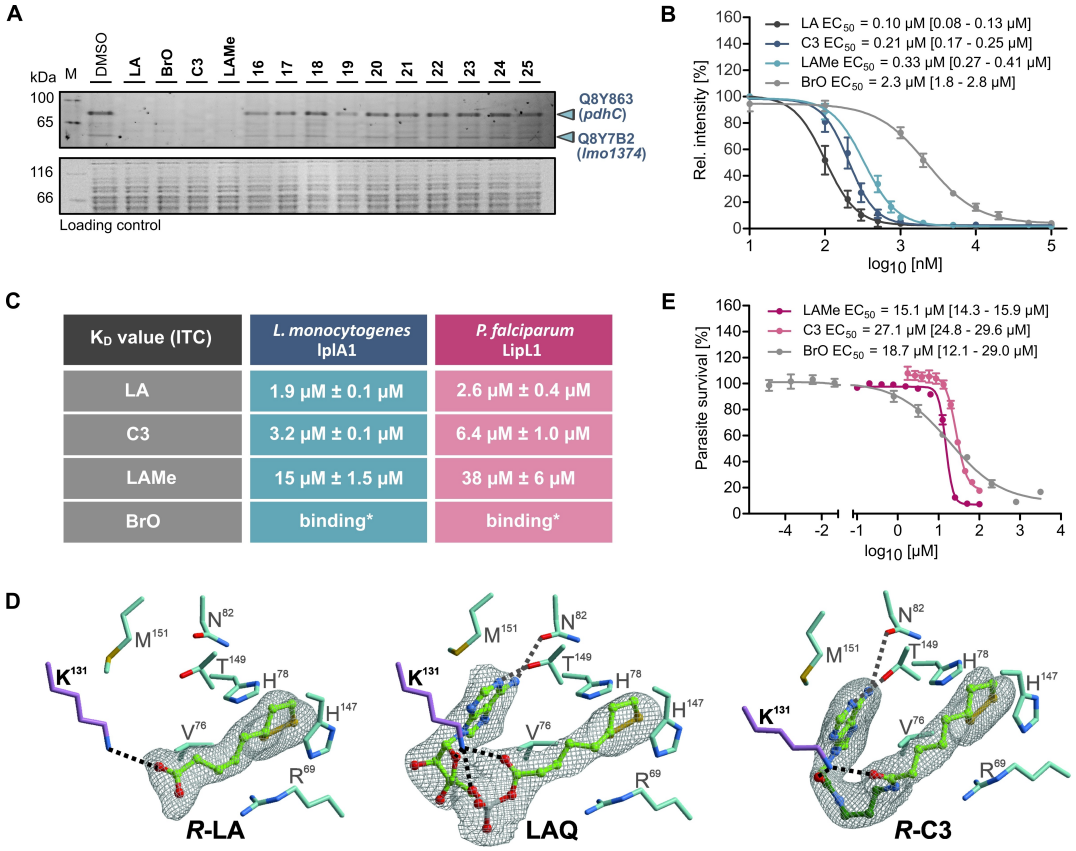


***Figure 4.*** Identification and validation of LPL inhibitors in *L. monocytogenes* (blue) and *P. falciparum* (magenta). A) A competitive screen of the 12 selected potential inhibitors in 10-fold excess (1 mM) compared to probe **2** (100 µM, 2 h) was performed in intact *L. monocytogenes* cells to identify cell-permeable LPL inhibitors by measuring the decreased fluorescent signals of reporter proteins. SDS-PAGE with fluorescent analysis was performed, and blue arrows indicate reporter proteins Q8Y863 (*pdhC*) and Q8Y7B2 (*lmo1374*). Coomassie stain served as loading control, and "M" indicates a protein marker. B) $EC_{50}$ value determination of corresponding gel-based in situ competitive labeling studies in *L. monocytogenes* cells with identified inhibitors **C3** and **LAMe** versus probe **2** (100 µM, 2 h). Fluorescent signal intensities for Q8Y863 (Figure S8A) were analyzed by ImageJ. The analysis, plotted with mean values and error bars indicating SEM, was performed in $n=3$ independent experiments, and competition with **LA** and **BrO** served as benchmarks. The error range is shown as 95% confidence interval. C) Recombinant *L. monocytogenes* lplA1 and *P. falciparum* LipL1 proteins were analyzed by ITC to separately verify the binding trends of inhibitors **C3** and **LAMe** towards LPL compared to **LA** and **BrO**. The experiments were measured at least in duplicates ($n\geq2$). Asterisk marks indicate qualitative ligand binding as low enthalpy change prevented quantification. D) Co-crystallization studies with *L. monocytogenes* lplA1 and ligands (*R*-**LA**, PDBID 8cri, left; **LAQ**, PDBID 8crj, middle; *R*-**C3**, PDBID 8crl, right) with respective $2F_O$-$F_C$ electron density maps (grey mesh, contoured to 1.0 σ) and amino acid interactions are depicted as a close-up of the active pocket. The analysis shows binding of *R*-**C3** as intermediate mimic with Lys131 (plume) as a key interaction for coordination of the lipoyl-domain and adenine unit. E) Blood-stage *P. falciparum* parasites were incubated in presence of **LAMe**, **C3**, and **BrO** concentration-dependently to measure parasite growth inhibition. Growth experiments were performed in quadruplicates ($n=4$) in two individual experiments. Mean values were plotted, and error bars represent SEM. The error range is shown as 95% confidence interval.

ligase of the parasite, demonstrating a comparably high binding affinity of **LA** ($K_D=2.6$ µM) and **C3** ($K_D=6.4$ µM) followed by **LAMe** ($K_D=38$ µM, Figure 4C, S10B). To evaluate the effects of **C3** and **LAMe** on the growth of **LA** auxotroph organisms, we tested the compounds against *L. monocytogenes* and *P. falciparum*. While we did not observe any effects on the growth of the bacterial strain, even in macrophage infection assays (Figure S12), **LAMe** and **C3** killed blood-stage *P. falciparum* with $EC_{50}$ values of 15 µM and 27 µM, respectively (Figure 4E). Although the benchmark inhibitor **BrO** achieved a similar $EC_{50}$ value, effective parasite eradication required millimolar concentrations, corroborating previous literature reports.[12a] Thus, these novel compounds represent the most potent LPL inhibitors reported to date.

## Conclusion

Lipoylation is a crucial post-translational modification which enables the catalysis of essential cellular processes, such as the oxidative decarboxylation of pyruvate to acetyl-CoA (pyruvate dehydrogenase).[8] As human and pathogenic cells differ in the salvage pathways for **LA**, selective inhibitors of pathogenic lipoate protein ligase represent an attractive strategy to develop anti-infective therapies.[13c] However,

tools to directly monitor LPL activity in living cells have been elusive so far.

We developed a cell-permeable lipoylation-probe (probe **2**) that utilizes LPL to modify **LA**-dependent enzymes covalently and thus serves as proxy for its activity. This in situ labeling strategy exhibits several benefits over screens against recombinant LPL, including the direct readout of cell permeability and sufficient in situ target engagement. Mass spectrometry confirmed the specificity of probe **2** for intracellular lysine residues in **LA**-dependent proteins. Based on this proof-of-concept, we designed a small virtual compound library by computational methods and identified two cell-permeable and potent active site LPL inhibitors, namely **C3** and **LAMe**. Co-crystallization of **C3** provided intriguing insights into LPL inhibition as the compound forms strong bonds with Lys131 in *L. monocytogenes* lplA1. However, no antibiotic activity was observed in *L. monocytogenes*, even though previous work showed that lplA1 is essential for the growth of bacteria in macrophages.[11a,b] We confirmed uptake and stability of **C3** in *L. monocytogenes*, raising the possibility that the lack of antibiotic activity could be due to strong competition with **LA** during salvage. Further modification of the inhibitor (e.g., mimicking the interaction of **LAQ** phosphate with Lys131 as observed in crystal structures) could improve competition with **LA**. Based on the conserved three-dimensional fold and active site pockets, we tested **C3** and **LAMe** against *P. falciparum* to see if these molecules may inhibit LPLs across species. Indeed, we saw killing of blood-stage parasites with both inhibitors, validating our approach.

Overall, we showcase LPL-dependent probes as ideal tools for identifying **LA** salvage pathway inhibitors with effective in situ activity against the malaria-causing parasite *P. falciparum.* As an outlook, iterative cycles of pre-selected computational compounds followed by intracellular LPL profiling will minimize the overall experimental effort and enhance the chances of cell-permeable hit molecules with high potency.

## Author Contributions

J.N.D. and S.A.S. conceived and designed the project. J.N.D. performed synthesis, labeling, mass spectrometry, protein purifications, ITC studies, and biological assays. S.Y.C. and M.H. ran docking studies and molecular dynamics simulations. M.G. performed crystallography with help of J.N.D. M.S. conducted assays with parasites in cell culture. S.M.H. provided isoDTB tags and assisted with the evaluation of binding site identification. S.A.S., J.N.D., and S.Y.C. wrote the manuscript with input of all authors.

## Acknowledgements

We acknowledge funding from the European Research Council (ERC) and the European Union's Horizon 2020 research and innovation program (grant agreement no. 725085, CHEMMINE, ERC consolidator grant) as well as from Merck KGaA Darmstadt (Merck Future Insight Prize 2020). We thank Prof. Dr. Kirsten Jung (LMU) for her kind donation of the *E. coli* Δ*lipB* knockout mutant (Keio collection) and Jonas Gellner (TUM) as well as Lennart Jona Brücher (TUM) for their help during synthesis. We also acknowledge input of PD Dr. Sven Halbedel (RKI) for macrophage infection assays. Further, we thank Astrid König (CPA) for excellent technical assistance in the crystallization experiments and the staff of the beamline X06SA at the Paul Scherrer Institute, Swiss Light Source (SLS), Villigen, Switzerland, for their help with data collection. We are grateful for the technical support offered by Mona Wolff (CPA), Laura Meier (CPA), and Katja Bäuml (CPA). Open Access funding enabled and organized by Projekt DEAL.

## Conflict of Interest

The authors declare no conflict of interest.

## Data Availability Statement

The proteomics data have been deposited to the ProteomeXchange Consortium[31] via the PRIDE[32] partner repository, which can be accessed with the identifier PXD040359. All new crystal structures have been deposited in the RCSB Protein Data Bank (PDB) with the depository numbers 8cri, 8crj, 8crl.[33] Analyzed proteomics data and comprehensive ZINC database[27] screen hits are presented in supplementary files.

**Keywords:** Anti-Infectives · Cofactors · Drug Discovery · Lipoic Acid · Proteomics

[1] A. Kirschning, *Angew. Chem. Int. Ed.* **2021**, *60*, 6242–6269.
[2] A. Ganesan, *Philos. Trans. R. Soc. B* **2018**, *373*, 20170069.
[3] a) A. Hoegl, M. B. Nodwell, V. C. Kirsch, N. C. Bach, M. Pfanzelt, M. Stahl, S. Schneider, S. A. Sieber, *Nat. Chem.* **2018**, *10*, 1234–1245; b) M. Pfanzelt, T. E. Maher, R. M. Absmeier, M. Schwarz, S. A. Sieber, *Angew. Chem. Int. Ed.* **2022**, *61*, e202117724.
[4] a) I. V. L. Wilkinson, M. Bottlinger, Y. El Harraoui, S. A. Sieber, *Angew. Chem. Int. Ed.* **2023**, *62*, e202212111; b) R. A. Homan, A. M. Jadhav, L. P. Conway, C. G. Parker, *J. Am. Chem. Soc.* **2022**, *144*, 15013–15019.
[5] a) M. J. Evans, B. F. Cravatt, *Chem. Rev.* **2006**, *106*, 3279–3301; b) B. F. Cravatt, A. T. Wright, J. W. Kozarich, *Annu. Rev. Biochem.* **2008**, *77*, 383–414; c) M. G. Paulick, M. Bogyo, *Curr. Opin. Genet. Dev.* **2008**, *18*, 97–106.
[6] I. V. L. Wilkinson, M. Pfanzelt, S. A. Sieber, *Angew. Chem. Int. Ed.* **2022**, *61*, e202201136.
[7] a) A. Solmonson, R. J. DeBerardinis, *J. Biol. Chem.* **2018**, *293*, 7522–7530; b) M. D. Spalding, S. T. Prigge, *Microbiol. Mol. Biol. Rev.* **2010**, *74*, 200–228; c) E. A. Rowland, C. K. Snowden, I. M. Cristea, *Curr. Opin. Chem. Biol.* **2018**, *42*, 76–85; d) J. E. Cronan, *Microbiol. Mol. Biol. Rev.* **2016**, *80*, 429–450.
[8] R. N. Perham, *Annu. Rev. Biochem.* **2000**, *69*, 961–1004.
[9] Q. H. Christensen, J. A. Hagar, M. X. D. O'Riordan, J. E. Cronan, *J. Biol. Chem.* **2011**, *286*, 31447–31456.

[10] a) J. E. Cronan, *Front. Genet.* **2020**, *11*, 510; b) X. Cao, L. Zhu, X. Song, Z. Hu, J. E. Cronan, *Proc. Natl. Acad. Sci. USA* **2018**, *115*, E7063–E7072.
[11] a) M. O'Riordan, M. A. Moors, D. A. Portnoy, *Science* **2003**, *302*, 462–464; b) K. M. Keeney, J. A. Stuckey, M. X. D. O'Riordan, *Mol. Microbiol.* **2007**, *66*, 758–770; c) K. Keeney, L. Colosi, W. Weber, M. O'Riordan, *J. Bacteriol.* **2009**, *191*, 2187–2196; d) J.-D. Sauer, A. A. Herskovits, M. X. D. O'Riordan, *Microbiol. Spectrum* **2019**, *7*, 7.4.26; e) R. J. Premaratne, W. J. Lin, E. A. Johnson, *Appl. Environ. Microbiol.* **1991**, *57*, 3046–3048.
[12] a) M. Allary, J. Z. Lu, L. Zhu, S. T. Prigge, *Mol. Microbiol.* **2007**, *63*, 1331–1344; b) C. Deschermeier, L.-S. Hecht, F. Bach, K. Rützel, R. R. Stanway, A. Nagel, F. Seeber, V. T. Heussler, *Cell. Microbiol.* **2012**, *14*, 416–430.
[13] a) S. L. Rei Yan, F. Wakasuqui, X. Du, M. R. Groves, C. Wrenger, *Front. Chem.* **2021**, *9*, 742175–742175; b) S. Günther, K. Matuschewski, S. Müller, *PLoS One* **2009**, *4*, e5510; c) J. Storm, S. Müller, *Curr. Pharm. Des.* **2012**, *18*, 3480–3489; d) C. Wrenger, S. Müller, *Mol. Microbiol.* **2004**, *53*, 103–113; e) S. C. Nair, J. T. Munro, A. Mann, M. Llinás, S. T. Prigge, *Proc. Natl. Acad. Sci. USA* **2023**, *120*, e2210929120.
[14] G. A. Afanador, K. A. Matthews, D. Bartee, J. E. Gisselberg, M. S. Walters, C. L. Freel Meyers, S. T. Prigge, *Mol. Microbiol.* **2014**, *94*, 156–171.
[15] B. Falkard, T. R. S. Kumar, L.-S. Hecht, K. A. Matthews, P. P. Henrich, S. Gulati, R. E. Lewis, M. J. Manary, E. A. Winzeler, P. Sinnis, S. T. Prigge, V. Heussler, C. Deschermeier, D. Fidock, *Cell. Microbiol.* **2013**, *15*, 1585–1604.
[16] M. J. Crawford, N. Thomsen-Zieger, M. Ray, J. Schachtner, D. S. Roos, F. Seeber, *EMBO J.* **2006**, *25*, 3214–3222.
[17] Q. Tang, Y. Guo, L. Meng, X. Chen, *Angew. Chem. Int. Ed.* **2021**, *60*, 4028–4033.
[18] S. Lai, Y. Chen, F. Yang, W. Xiao, Y. Liu, C. Wang, *J. Am. Chem. Soc.* **2022**, *144*, 10320–10329.
[19] M. Fernández-Suárez, H. Baruah, L. Martínez-Hernández, K. T. Xie, J. M. Baskin, C. R. Bertozzi, A. Y. Ting, *Nat. Biotechnol.* **2007**, *25*, 1483–1487.
[20] W. Zhong, B. Sun, C. Lu, H. Yu, C. Wang, L. He, J. Gu, S. Chen, Y. Liu, X. Jing, Z. Bi, G. Yang, H. Zhou, T. Sun, C. Yang, *Sci. Rep.* **2016**, *6*, 35579.
[21] L. Tan, S. Maji, C. Mattheis, Y. Chen, S. Agarwal, *Macromol. Biosci.* **2012**, *12*, 1721–1730.
[22] K. Fujiwara, S. Toma, K. Okamura-Ikeda, Y. Motokawa, A. Nakagawa, H. Taniguchi, *J. Biol. Chem.* **2005**, *280*, 33645–33651.
[23] P. R. A. Zanon, L. Lewald, S. M. Hacker, *Angew. Chem. Int. Ed.* **2020**, *59*, 2829–2836.
[24] UniProt Consortium, *Nucleic Acids Res.* **2023**, *51*, D523–D531.
[25] a) K. Fujiwara, N. Maita, H. Hosaka, K. Okamura-Ikeda, A. Nakagawa, H. Taniguchi, *J. Biol. Chem.* **2010**, *285*, 9971–9980; b) A. J. Guerra, G. A. Afanador, S. T. Prigge, *Proteins Struct. Funct. Bioinf.* **2017**, *85*, 1777–1783.
[26] M. Mirdita, K. Schütze, Y. Moriwaki, L. Heo, S. Ovchinnikov, M. Steinegger, *Nat. Methods* **2022**, *19*, 679–682.
[27] J. J. Irwin, T. Sterling, M. M. Mysinger, E. S. Bolstad, R. G. Coleman, *J. Chem. Inf. Model.* **2012**, *52*, 1757–1768.
[28] D. R. Koes, C. J. Camacho, *Nucleic Acids Res.* **2012**, *40*, W409–W414.
[29] J. Feng, A. S. Paparella, G. W. Booker, S. W. Polyak, A. D. Abell, *Antibiotics* **2016**, *5*, 26.
[30] J. Feng, A. S. Paparella, W. Tieu, D. Heim, S. Clark, A. Hayes, G. W. Booker, S. W. Polyak, A. D. Abell, *ACS Med. Chem. Lett.* **2016**, *7*, 1068–1072.
[31] J. A. Vizcaíno, E. W. Deutsch, R. Wang, A. Csordas, F. Reisinger, D. Ríos, J. A. Dianes, Z. Sun, T. Farrah, N. Bandeira, P.-A. Binz, I. Xenarios, M. Eisenacher, G. Mayer, L. Gatto, A. Campos, R. J. Chalkley, H.-J. Kraus, J. P. Albar, S. Martinez-Bartolomé, R. Apweiler, G. S. Omenn, L. Martens, A. R. Jones, H. Hermjakob, *Nat. Biotechnol.* **2014**, *32*, 223–226.
[32] Y. Perez-Riverol, A. Csordas, J. Bai, M. Bernal-Llinares, S. Hewapathirana, D. J. Kundu, A. Inuganti, J. Griss, G. Mayer, M. Eisenacher, E. Pérez, J. Uszkoreit, J. Pfeuffer, T. Sachsenberg, Ş. Yılmaz, S. Tiwary, J. Cox, E. Audain, M. Walzer, A. F. Jarnuczak, T. Ternent, A. Brazma, J. A. Vizcaíno, *Nucleic Acids Res.* **2019**, *47*, D442–D450.
[33] H. M. Berman, J. Westbrook, Z. Feng, G. Gilliland, T. N. Bhat, H. Weissig, I. N. Shindyalov, P. E. Bourne, *Nucleic Acids Res.* **2000**, *28*, 235–242.

Manuscript received: April 3, 2023
Accepted manuscript online: May 30, 2023
Version of record online: June 26, 2023